PCCP

Accepted Manuscript

ROYAL SOCIETY OF CHEMISTRY

www.rsc.org/pccp

Interaction of Gas Phase Oxalic Acid with Ammonia and Its Atmospheric Implication

Xiu-Qiu Peng,[1,2] Yi-Rong Liu,[1] Teng Huang,[1] Shuai Jiang,[1] Wei Huang[1,2]*

[1]*Laboratory of Atmospheric Physico-Chemistry, Anhui Institute of Optics & Fine Mechanics, Chinese Academy of Sciences, Hefei, Anhui 230031, China*

[2]*School of Environmental Science & Optoelectronic Technology, University of Science and Technology of China, Hefei, Anhui 230026, China*

*E-mail: huangwei6@ustc.edu.cn

Abstract

Oxalic acid is believed to play an important role in the formation and growth of atmospheric organic aerosols. However, as common organic acid, the understanding of the larger clusters formed by gas phase oxalic acid with more ammonia molecules is incomplete. In this work, the structural characteristics and thermodynamics of oxalic acid clusters with up to six ammonia molecules have been investigated at the PW91PW91/6-311++G(3df,3pd) level of theory. We found that oxalic acid form relatively stable clusters with ammonia molecules, and the ionization events play a key role. The analyses of thermodynamics and atmospheric relevance indicate the heterodimer $(H_2C_2O_4)(NH_3)$ show relative obvious concentration in the atmosphere, thus they likely participate in new particle formation. But with the increase of the number of ammonia, the concentration of clusters decreases gradually. Additionally, clusters of oxalic acid with ammonia molecules are predicted to form favorably in low temperature condition and show high Rayleigh scattering intensities.

INTRODUCTION

Atmospheric aerosols are known to be involved in many important processes, including changing the Earth's climate by modifying cloud precipitation and properties,[1, 2] influencing the Earth's radiation budget by absorbing and scattering solar radiation, affecting human health and, possibly, enhancing mortality rate (e.g., by particles less than 2.5 μm).[3-5] New particles formation (NPF) produces a majority of atmospheric aerosols.[6] In the past, a mountain of theoretical and experimental work are focused on NPF event to investigate the properties and structures of the molecular clusters,[7-21] and both methods have provided valuable perception of the potential chemical mechanisms of particle formation. The formation of new particles involves two stages.[22-25] An initial nucleation stage form critical nucleus (~1-3 nm in diameter) and a subsequent growth stage where the size of critical clusters increase rapidly.[24, 26] The initial stage is critical and important that its chemical makeup and population would affect the NPF event along with the nucleation rate. So far, the chemical compositions of the critical nucleus and the identity of chemical species that participate in NPF still remains uncertainty related to aerosol production.

Among these studies, the nucleation of organic matter with sulfuric acid, water and ammonia, the dominant nucleating species in the atmosphere, has received increasing amounts of attention. As is known, organic acids generally exist in nature and play an important role in ice nucleation,[27-30] cloud condensation,[31] and the production of fine particulate matter.[32, 33] The pioneering laboratory experiments on nucleation of organic acids by Zhang *et al.* and the theoretical study of Yu *et al.* have

clearly shown that organic acids enhance the nucleation and growth of nanoparticles involving sulfuric acid.[34, 35] Previously, Nadykto and Yu indicated that both organic acids and ammonia may efficiently stabilize the binary H_2SO_4-H_2O clusters and that the organic acids actively interact with ammonia.[36] As the most common dicarboxylic acid in the Earth's atmosphere,[37-40] oxalic acid has been observed with a significant concentration and is the dominant organic acid found in the $PM_{2.5}$ atmospheric aerosols.[41, 42] Furthermore, the analysis of the field measurements[43] revealed a strong correlation between the Cloud Condensation Nuclei (CCN) and oxalate concentrations, which indicated that oxalate may play an important role in the CCN activation. Zhang *et al.* showed that dicarboxylic acids can contribute to the aerosol nucleation process by binding to sulfuric acid and ammonia.[6] The theoretical investigation of Yu *et al.* predicted that oxalic acid significantly enhances the stability of ionic clusters, catalyzing prenucleation clusters with positive charges.[44] Moreover, Tao *et al*.[45] reported that the formation of neutral cores is the most important step in the initial formation of oxalic acid and water clusters; recently, they predicted that $H_2C_2O_4$-NH_3 core thermodynamically stable clusters may likely participate in NPF chemistry and their subsequent hydration are favored compared to the monohydrates of oxalic acid.[46] The significance of $H_2C_2O_4$-NH_3 core to the subsequent hydration in the atmosphere is clear, however, what possible features could the clusters of oxalic acid with ammonia show in larger size? If the clusters of oxalic acid with ammonia in larger size indicate stable in structures and a certain concentration similar to $H_2C_2O_4$-NH_3 core, these clusters may exist in the atmosphere and participate in the

subsequent hydration. Thus, it is of interest and necessary to study the clusters of oxalic acid with more ammonia molecules. In this work, we investigate the initial ionization events of $(H_2C_2O_4)(NH_3)_n$ (n=1~6), its atmospheric relevance, temperature dependence and the Rayleigh light scattering properties at the molecular level. The structure and energies of clusters $(H_2C_2O_4)(NH_3)_n$ (n=1~6) are predicted using basin-hopping (BH) method[47-49] coupled with density functional theory (DFT) calculation. To the best of our knowledge, there is no similar research on the ability of the BH global searching method to search for the low-lying isomers of $(H_2C_2O_4)(NH_3)_n$ clusters. The BH approach was tested to be highly efficient for many atomic clusters, such as gold clusters,[50-53] boron clusters[54] and doped gold clusters.[55] A new sampling skill called compressed sampling was effectively introduced to BH coupled with DFT and verified by water, nitrate-water, oxalate-water clusters and chlorine-water clusters.[56-58]

THEORETICAL METHODS

The initial geometries of monomers and $(H_2C_2O_4)(NH_3)_n$ (n = 1~6) clusters in this study were searched using the BH method coupled with DFT. Generalized gradient approximation in the Perdue-Burke-Ernzerhof (PBE) functional and the double numerical plus d-functions (DND) basis set, implemented in DMol3,[59] were chosen for the structure optimization of this system. This method has been used to explore the atomic and molecular systems by our previous studies. [49, 53-55, 57,58,60-62]

For each cluster, three separate BH searches, consisting of 1000 sampling steps at 3000K starting with randomly generated molecular configurations, were performed.

The geometries were first optimized at PW91PW91/6-31+G* level of theory. The isomers located within 6 kcal mol^{-1} of the global minimum are then selected and reoptimized by the PW91PW91/6-311++G(3df,3pd) level of theory implemented in the Gaussian 09 software package[63]. The PW91PW91 method has shown fine performance on clusters containing common organic acids, and its predictions[36, 44] agree best with experiments compared to other density functionals. In order to make sure the results are consistent, another four methods (ω B97x-D, M06-2X, CAM-B3LYP and B3LYP) were performed for the smallest clusters including NH_3, $C_2O_2H_4$, $(C_2O_2H_4)(NH_3)$ and $(C_2O_2H_4)(NH_3)_2$. We choose to use density functional instead of wave function theory methods (i.e. MP2) to compare with each other like the work by Elm *et al.* [20] On one hand, the computational costs could be largely reduced due to the absence of wave function theory. And on the other hand, the accuracy of benchmark could be maintained because recent benchmark articles[19, 20] provide the pool of potential density functional methods including those methods mentioned in this benchmark work. From the current benchmark work displayed in Table 1, Gibbs free energy calculated by PW91 was closer to M06-2X and ωB97x-D, rather than CAM-B3LYP and B3LYP. In cluster $(C_2O_2H_4)(NH_3)$, free energy changes calculated by PW91PW91 was very close to that calculated by M06-2X: the results were -4.172 kcal mol^{-1} and -3.324 kcal mol^{-1}, respectively. The differences between free energy changes calculated by PW91PW91 and free energy changes calculated by ωB97x-D were 1.75 kcal mol^{-1}. In cluster $(C_2O_2H_4)(NH_3)_2$, the differences between free energy changes calculated by PW91PW91 with other methods increased, but near

3 kcal mol^{-1}, this could be acceptable as the differences among different functional results are supposed to increase with the increasing size of clusters.

For each stationary point, frequency calculations were confirmed that no imaginary frequencies existed (Details can be seen in the supporting information). The single-point energies of the selected isomers of the $(H_2C_2O_4)(NH_3)_n$ (n=1~6) system were ultimately calculated at DF-MP2-F12/vdz-f12 level of theory using Molpro 2010.1,[64, 65] and this level of theory has been proved to be accurate for the single-point energies calculations for $(C_2O_2H_4)(H_2SO_4)_2(H_2O)_n$ (n=1~3) and $(C_2O_2H_4)(HSO_4^-)(H_2SO_4)(H_2O)_n$ (n=1~3)systems.[62] The relative energies (ΔE_{rel}) were defined as the relative electronic energy of the global minimum. The ZPE-corrected binding energies (ΔE_0) and the relative energies (ΔE_{rel}) are obtained at a standard state of 0K and 1 atm. Intermolecular enthalpies (ΔH) and Gibbs free energies (ΔG) were calculated at a temperature of 298.15 K and 1 atm. Subsequently, to better clarify the nature of the intramolecular hydrogen bond interactions of clusters in various size, the characteristics of bond critical points (BCPs) were analyzed using the atoms in molecules (AIM)[66] approach by means of Multiwfn program.[67] To study non-covalent interaction (NCI) of oxalic acid with ammonia, the reduced density gradient (RDG) associated with the hydrogen binding regions in real space have been calculated using the Multiwfn program and visualized with the VMD program.[68] The RDG method presented by Yang and coworkers[69] has been validated to be convenient and effective for identifying the non-covalent interaction.

To evaluate the Rayleigh scattering intensities and polarization ratios of oxalic

acid with ammonia, the most common dicarboxylic acid and the dominant base in the atmosphere, the binding mean isotropic and anisotropic polarizabilities of all clusters have been calculated at CAM-B3LYP/aug-cc-pVDZ level of theory. The benchmark work of the smallest cluster subunits H_2SO_4, NH_3 and H_2O was performed by Elm *et al.*[70] On the basis of this analysis, they found that CAM-B3LYP/aug-cc-pVDZ was a good compromise between efficiency and accuracy yielding good agreement with both experimental and CCSD(T) values of the polarizability. Furthermore the CAM-B3LYP functional has been successfully used in the calculation of various response properties such as polarizabilities,[71, 72] absorption properties,[73] van der Waals C_6-coefficients,[71] and magnetic circular dichroism.[74, 75] Additionally, CAM-B3LYP showed an adequate performance in calculating the hyper Rayleigh scattering of large chromophores.[76] In this article, to find a suitable methodology for calculating the optical properties of pre-nucleation clusters, a DFT functional with aug-cc-pVDZ basis set analysis was performed for the smallest clusters including NH_3, $C_2O_2H_4$, $(C_2O_2H_4)(NH_3)$ and $(C_2O_2H_4)(NH_3)_2$. The performance of calculating the mean isotropic polarizability was tested using ωB97x-D, M06-2X, MP2, CAM-B3LYP and PW91 with aug-cc-pVDZ basis set. The results were shown in Table 2, on the analysis of the results, CAM-B3LYP/aug-cc-pVDZ was found to be a good compromise between accuracy and efficiency yielding good agreement with MP2 values of the polarizability.

Light scattering intensities and the isotropic mean polarizabilities $\bar{\alpha}$ as well as anisotropic polarizabilities $\Delta\alpha$,the relevant computation methods have been given in

our previous study.[58]

RESULTS AND DISCUSSION

3.1 Structures and Energies

The geometry of the oxalic acid monomer in this work is a planar *trans* conformation (C_{2h} point group), with weak intramolecular hydrogen bonds to the carboxyl oxygen at neighboring carboxyl groups.[6, 44] The representations of $(H_2C_2O_4)(NH_3)_n$ (n=1~6) conformations were defined using m-n notation. In this notation, "m" (m = I, II, III, IV, V and VI) denoted the number of ammonia molecules. "n" (n = a~d) was used to distinguish different isomer with the same value of m, ordered by the increasing relative single point energy ΔE_{rel}. The ZPE-corrected binding energies (ΔE_0) of the cluster were calculated using the following equation. Interaction enthalpies (ΔH) and free energy changes (ΔG) were calculated at the same way:

$$\Delta E_n = E_n - n \times E_{NH_3} - E_{C_2O_4H_2} \quad (1)$$

where n indicates the ammonia number in the cluster, E_n is the total energy; E_{NH_3} and $E_{C_2O_4H_2}$ are the total energy for ammonia and oxalic acid. The binding energies of all isomers are shown in Table 3. The most stable structure of the $H_2C_2O_4$-NH_3 isomers was consistent with the available reported structure.[45, 46]

Fig.1 displays structures optimized of the global and local minima at PW91PW91/6-311++G(3df,3pd) level of theory for $(H_2C_2O_4)(NH_3)_n$. The lowest-energy structures of the $(H_2C_2O_4)(NH_3)_n$ (n=1~6) clusters are ordered by the

state of dissociation (I, II, III, IV, V and VI). Isomers with ammonia binding to either carboxyl and with the relative single point energy above 6 kcal mol^{-1} were displayed in Figure. S1, the corresponding binding energies were shown in Table S1 (Details can be seen in the supporting information). The intramolecular and intermolecular interaction distances and the corresponding isosurfaces are given in Fig.2. For the $H_2C_2O_4$-NH_3 complexes, the global minimum of the $H_2C_2O_4$-NH_3 cluster is I-a. From Fig.2, two intermolecular hydrogen bonds are formed in cluster I-a, a stronger H···N bond with the length of 1.536 Å and a weaker O···H bond with the length of 2.154 Å. In $(H_2C_2O_4)(NH_3)_2$ clusters, the global minimum is II-a. It is observed that the length of the stronger intermolecular H···N bond reduces to 1.211 Å from 1.536 Å, the length of the adjacent covalent O-H bond increases from 1.067 Å to 1.304 Å. The global minimum of $(H_2C_2O_4)(NH_3)_3$ clusters is III-a, with a enthalpy change ΔH= -36.219 kcal mol^{-1},and free energy change ΔG= -6.018 kcal mol^{-1}. The addition of the second ammonia produces a free energy change of 2.743 kcal mol^{-1} higher than that of $(H_2C_2O_4)(NH_3)$, however, the addition of the third ammonia produces a free energy change of -3.614 kcal mol^{-1} lower compared to that of $(H_2C_2O_4)(NH_3)_2$. In this configuration, a proton of the donor $H_2C_2O_4$ transfers to the accepter ammonia, the length of the strong intermolecular H···N bond reduces to 1.097 Å, nearly to the nitrogen hydrogen bond distances of ammonia. The length of the adjacent covalent O-H bond increases from 1.304 Å to 1.538 Å, forming an ion pair of $HC_2O_4^-/NH_4^+$. For the clusters of $(H_2C_2O_4)(NH_3)_n$ (n=4~6), the distance of intermolecular H···N bonds decreases with the clusters grow to larger size. In clusters $(H_2C_2O_4)(NH_3)_4$, part

of the free energy change are negative, some are positive. For the clusters of $(H_2C_2O_4)(NH_3)_n$ (n=5~6), the free energy change are all positive. This indicates ionization events exist in the formation of $(H_2C_2O_4)(NH_3)_n$ cluster and play a role on the stability of oxalic acid and ammonia system, furthermore, three ammonia molecules are needed for oxalic acid dissociation.

3.2. Electron Density and Non-Covalent Interactions (NCI) Analysis.

The topological analysis of the electron density can prove the existences of the hydrogen bond in all clusters. So AIM theory[66] was applied here to deepen the nature of the intermolecular hydrogen bond between oxalic acid and ammonia system. To analyze the topological characteristics at the bond critical point, we used the electron density (ρ), its Laplacian ($\nabla^2\rho$), and the electronic energy density (E), which is composed of the electronic kinetic energy density (G) and the electronic potential energy density (V). ρ is a good estimate of the strength of hydrogen bond.[66] The larger the ρ value, the stronger the hydrogen bond is. The values of AIM topological parameters calculated using the Multiwfn program[67] of the hydrogen bonds between $H_2C_2O_4$ and NH_3 for all global minima are listed in Table 4. It indicates hydrogen-bonded intermolecular interactions exsit in these complexes. And some intermolecular hydrogen bonds are relative strong. The values of $\nabla^2\rho$ and E indicate the nature of the interaction. A negative value of $\nabla^2\rho$ indicates that there is a shared interaction, such as in a covalent bond, whereas a positive value of $\nabla^2\rho$ indicates closed-shell system interactions, that is, ionic interactions, van der Waals forces, or hydrogen bonding.[66] On the other hand, if $\nabla^2\rho$ is positive but E is negative, then the

interaction is partly covalent in nature.[77] Here -G/V is chosen as the balance between the positive value of G and the negative value of V may indicate the regions corresponding to covalent or non-covalent interactions. If -G/V is greater than 1, then the interaction is non-covalent. If the ratio is between 0.5 and 1, the interaction is partly covalent in nature, and when this ratio is less than 0.5, the interaction is a shared covalent interaction.[78] The global minima with hydrogen bond distances and corresponding isosurfaces are shown in Fig.2. From Fig.2 and Table 4, the length of the intermolecular stronger H···N bond of $(H_2C_2O_4)(NH_3)_n$ (n=1~6) clusters decays from 1.536 Å to 1.055 Å. The relevant value of ρ increases from 0.0853 a.u. to 0.3338 a.u. The interaction in this H···N bond with −G/V=0.52 is partly covalent in the dimer, then tending to shared covalent in trimer. The coterminous O···H bond increases from 1.067 Å to 1.735 Å. The relevant value of ρ decays from 0.2671 a.u. to 0.0446 a.u.. The interaction in this O···H bond with −G/V=0.14 is covalent in the dimer, then beginning close to partly covalent from trimer and resulting in hydrogen bond till tetramer. From these values, the tetramer can be seen as a turning point of the proton transfer, verifying the former structures analysis. The −G/V values of other hydrogen bonds forming of oxalic acid and ammonia are greater than 1, and these interactions are non-covalent. The relevant value of ρ ranges from 0.0106 a.u. to 0.0225 a.u., which fall in the generally accepted range of a hydrogen bond, which is in the range of (0.002 to 0.035) a.u., and their corresponding Laplacian ($\nabla^2\rho$, all fall in the proposed range of (0.024 to 0.139) a.u. of a hydrogen bond,[79] showing that there are hydrogen-bonded intermolecular interactions of oxalic acid and ammonia system.

The non-covalent interaction (NCI) index based on the correlation between the reduced density gradient and the electron density has been presented by Yang and coworkers.[69, 80] The reduced density gradient

$$s = \frac{1}{2(3\pi^2)^{1/3}} \frac{|\nabla\rho|}{\rho^{4/3}} \quad (2)$$

is a fundamental dimensionless quantity in DFT, which is used to describe the deviation from a homogeneous electron distribution.[69, 81] To some extent, the NCI analysis method can be seen as an extension of AIM.[80] Not only can the location of the pairwise atoms connected along the bond path be identified, but also the properties around BCPs can be visualized using NCI. The reduced density gradient is able to be used to confirm the non-covalent interactions and covalent interactions in real space.[82] Therefore, the NCI index is a useful tool to distinguish and visualize different types of non-covalent interactions as regions of real space. If the color coding of the bonding isosurface is from green to blue, indicating that the hydrogen-bonded interaction is becoming stronger. The reduced gradient isosurface (s = 0.05 a.u.) (using the Multiwfn program[67] and VMD program[68]) of Fig.2 agrees with the analysis of AIM. In the middle region of the intermolecular nitrogen and hydrogen atoms, the intermolecular oxygen and hydrogen atoms, as well as the intramolecular oxygen and hydrogen atoms, there exist bonding isosurfaces. Here, it is observed that both intermolecular stronger and weaker hydrogen bondings exist in oxalic acid and ammonia system. Some intermolecular hydrogen bondings are relative stronger. From Fig.2, the phenomenon of the proton transfer can also be seen. Proton transfer occurs in the tetramer, and which consistent with the results of AIM.

3.3 Temperature Dependence of Conformational Populations

From the previous studies,[58] as the systems grow larger and form more complex, the stability order of isomers may change. Temperature effects could also contribute to the population order variation of isomers. Thus the temperature dependence of thermodynamic properties is an important parameter to understand the roles of specific nucleation mechanisms at various atmospheric temperatures. Experiments at lower temperature ranges are difficult to perform due to the increased wall losses of the clusters ($H_2C_2O_4$ and NH_3) at low temperatures. Here quantum chemical calculations can provide such data. In this work, the temperature dependence of energy for the formation of $H_2C_2O_4$ and NH_3 complexes was calculated at temperatures of 100, 150, 200, 250, 298.15, 300, 350 and 400 K.

Considering the Boltzmann distribution of the lower energy isomers, here we used the Boltzmann averaged Gibbs free energy to study the flatness of the potential energy surface of $(H_2C_2O_4)(NH_3)_n$ (n = 1~6). The equations are listed in follows:

$$\eta_n^i = \frac{e^{\frac{-\Delta\Delta G_n^i}{k_B T}}}{\sum_i e^{\frac{-\Delta\Delta G_n^i}{k_B T}}} \quad (3)$$

$$\Delta G_n = \sum_i \eta_n^i \Delta G_n^i \quad (4)$$

Where

$$\Delta G_n^i = G_n^i - G^{C_2O_4H_2} - nG^{NH_3} \quad (5)$$

$$\Delta\Delta G_n^i = \Delta G_n^i - \min\left\{\Delta G_n^i\right\} \quad (6)$$

Here *i* and *n* represent the isomer order in a cluster and the number of NH_3 respectively. The temperature dependence of the conformational population shown for

n = 4, n = 5 and n = 6 is shown in Fig. 3~5, respectively. It is obvious that the global minimum has the greatest weight in the ensemble of energetically accessible conformers at the range of 100K to 400K. As temperature increases, the weight of the global minimum decreases, and the roles of other local minima become competitive.

For n = 4 (Fig.3), the global minimum IV-a carries the highest weight, but the weigh has a declining trend from 100 K to 400 K. The conformation population of the isomer IV-b increases with the increasing temperature, but is still below the global minimum at 400 K; further investigation is required to determine whether this isomer competes with the global minimum at temperatures above 400 K. The conformational populations of isomers IV-c increase with increasing temperature up to 300 K and then decrease as the temperature further increases to 400 K. The isomers of IV-e, IV-f, IV-g and IV-h have similar trends to IV-d. In addition, the electronic energy effect can be seen from the competing role of these isomers.

For n = 5 (Fig. 4), the global minimum V-a weighs more than other low-lying isomers below temperatures of approximately 400 K. Below 200 K, the conformational populations of both V-c and V-d weigh less than V-b; however, the trend is reversed when temperature exceeds 200 K. In addition, the electronic energy effect can be observed from the competing roles of V-c and V-d because their electronic energies are quite close to the global minimum (energy differences of 1.04 kcal mol^{-1} and 1.232 kcal mol^{-1}, respectively).

For n = 6 (Fig. 5), the competitive local minima (VI-b) are more weighed than other local minima when the temperature above 150 K , and its proportion increases

with the increasing temperature. Other isomers, VI-c, VI-d,VI-e and VI-f have the same trend from 100K to 400K.

The Gibbs free energy of $(H_2C_2O_4)(NH_3)_n$ (n = 4~6) at different temperatures proves that the coupling of the contributions of various isomers and temperature effects could change the relative stabilities of $(H_2C_2O_4)(NH_3)_n$ (n = 4~6). The present study focuses on $(H_2C_2O_4)(NH_3)_n$ clusters, so no H_2O molecules were included in the complex models. Although H_2O molecules are not included in the calculations, the present work still provides important information for the understanding of cluster formation processes from NH_3 and $H_2C_2O_4$ molecules. Investigation of H_2O effects are part of our future research.

3.4 Thermodynamics of Cluster Formation

Thermodynamic analyses can provide insight into the realizability and possibility of clusters formation. Gibbs free energy changes are used for evaluating the strength of the intermolecular interaction and the spontaneity in the process of the clusters formation. As shown in Table 3, the calculated thermodynamic parameters (ZPE-corrected binding energies at 0K, enthalpies and Gibbs free energy changes at 298.15K) for n = 1~6 clusters are acquired by thermal corrections using the PW91PW91 correction and single point electronic energies from DF-MP2-F12 theory as described in the methods section. From Table 3 we see that the heterodimer of oxalic acid and ammonia is exothermic by 14.094 kcal mol^{-1}, and the trimer of one oxalic acid with two ammonia molecules is exothermic by 20.539 kcal mol^{-1}. The formation of a cluster containing one oxalic acid and three ammonia molecules is

exothermic by 28-34 kcal mol^{-1}, and 32-37 kcal mol^{-1} is released during the formation of the $(H_2C_2O_4)(NH_3)_4$ cluster. For the formation of $(H_2C_2O_4)(NH_3)_5$ and $(H_2C_2O_4)(NH_3)_6$ clusters, 40-44 kcal mol^{-1} and 45-51 kcal mol^{-1} are released, respectively. The calculation results of Gibbs free energies at room temperature are as follows: -5.147 kcal mol^{-1} for the dimerization of one oxalic acid with one ammonia molecule, -2.404 kcal mol^{-1} for the trimerization of one oxalic acid with two ammonia molecules, -1.405~-6.018 kcal mol^{-1} for the $(H_2C_2O_4)(NH_3)_3$ cluster, -1.449~3.405 kcal mol^{-1} for the $(H_2C_2O_4)(NH_3)_4$ cluster, 0.522~3.470 kcal mol^{-1} for the $(H_2C_2O_4)(NH_3)_5$ cluster, and 3.495~9.129 kcal mol^{-1} for the $(H_2C_2O_4)(NH_3)_6$ cluster. The Boltzmann averaged Gibbs energies for the formation of $(H_2C_2O_4)(NH_3)_n$ clusters are displayed in Table 3. At room temperature, the Gibbs free energies of the clusters range from -6.297 kcal mol^{-1} for the dimerization to 9.129 kcal mol^{-1} for the formation of the $(H_2C_2O_4)(NH_3)_n$ (n=1~6)cluster. Clearly, thermodynamics favors the formation of oxalic acid with up to four ammonia molecules at room temperature.

Additionally, in Fig. 6, ΔG from the global minimum of $(H_2C_2O_4)(NH_3)_n$ (n=1~6) cluster increases throughout the temperature range from 100K to 400K, this may predict the stability of the global minima becomes lower with the increasing temperature. On the other hand, these clusters may form favored in low temperature condition.

3.5 Atmospheric Relevance

Determining the concentrations of the various oxalic acid with ammonia clusters under a given realistic atmospheric condition is of interest. The concentrations can

provide a possible reference for the existence in the atmosphere of corresponding clusters. Briefly, the equilibrium constants K_n for the formation of the clusters from the respective monomers were calculated from the standard free energies ($\Delta G_{298.15\ K}$) using relation (7):

$$\Delta G = -RT\ln(K_n) \quad (7)$$

For reaction (8), the corresponding equilibrium constant K_n is defined by relation (9):

$$H_2C_2O_4 + nNH_3 \leftrightarrow H_2C_2O_4 \cdot nNH_3 \quad (8)$$

$$K_n = \frac{[C_2O_4H_2 \cdot nNH_3]}{[NH_3]^n[C_2O_4H_2]} \quad (9)$$

A quantity referred to the relative population fraction (RPF) is then defined by relation (10):

$$RPF = \frac{[C_2O_4H_2 \cdot nNH_3]}{[C_2O_4H_2]} = K_n[NH_3]^n \quad (10)$$

The total concentrations of ammonia and oxalic acid were chosen to be 1 and 5 ppb, respectively;[45, 46] both of these values correspond to typical and reasonable concentrations of these pollutant species. These calculations were performed for all clusters, and the results are listed in Table 5. The $H_2C_2O_4$-NH_3 clusters are predicted to have a concentration of 8.02×10^5 molecules cm^{-3} in the atmosphere. Clearly, the real situation in the atmosphere is much more complicated, and these calculations represent a simplistic and limited approximation. However, these results provide a general estimation of the importance of various clusters. Table 5 also shows the relative population fractions (RPF) calculated at 298.15 K for $(H_2C_2O_4)(NH_3)_n$

(n=1~4). From the results of $(H_2C_2O_4)(NH_3)_3$ and $(H_2C_2O_4)(NH_3)_4$, it seems that the lower energy forms of the clusters are usually more effective binders of ammonia, and their relatively higher populations make them more contributions to the atmospheric population. However, the concentrations of the clusters gradually decrease while binding more ammonia molecules. They are found in concentrations 10^6-10^{12} fold more dilute. Especially for n=4, clusters show infinitesimal populations at typical boundary layer atmospheric temperatures, this could be due to the relative lower concentration of ammonia than oxalic acid in the atmosphere.

3.6 Optical properties

Aerosols weaken the light by scattering and absorbing, the extinction properties have great impact on atmospheric visibility and radiative forcing.[83, 84] The light scattering properties of particles, clusters and molecules in atmosphere are related to the wavelength of the incoming light and their size. While the diameters much lower than the wavelength of the incoming radiation, Rayleigh scattering is the dominant mechanism.[70, 85, 86] Jonas Elm and his co-workers found the Rayleigh scattering intensity depends quadratically on the number of water molecules in clusters, and even a single ammonia molecule is able to induce a high anisotropy, which further increases the scattering intensity.[70] Additionally, Rayleigh scattering is also used to analyse hydrogen-bonded systems with *ab initio* calculations.[87-90]

Depolarization ratios and Rayleigh scattering intensities for the perpendicular and parallel components of linear polarized light for $(H_2C_2O_4)(NH_3)_n$ systems are calculated at the level of CAM-B3LYP/aug-cc-pVDZ. The isotropic mean

polarizabilities $\bar{\alpha}$ are quite size dependent and vary linearly with correlation coefficient $\rho = 0.99986$ as shown in Fig. 7(c), consistent with the study of methanol clusters and chloride hydration clusters.[58, 90] In Fig. 7, the Rayleigh light scattering intensity of natural light $\Re_n$ and the depolarization ratios ρ_n of the $(H_2C_2O_4)(NH_3)_n$ clusters can be seen as a function of the number of ammonia molecules in the cluster. The non-linear dependence of $\Re_n$ on the number of ammonia molecules is observed to closely follow the trend of a second order polynomial, consistent with the results of sulfuric acid hydration systems and chloride hydration systems.[58, 70] This increasing trend can be attributed to the gradually increasing binding polarizability of the clusters, such that the $(\bar{\alpha})^2$ term in equation (6) will dominate in the Rayleigh scattering of larger particles. The calculated depolarization ratios ρ_n are observed to decay as the cluster grows. This is due to the increase in the mean isotropic polarizability with the number of molecules in combination with the anisotropic polarizability being relatively constant in the range of 27–35 a.u. This is consistent with what is to be expected as the clusters change from a molecular cluster into a spherical isotropic particle. Additionally, the depolarization ratios for clusters with 1~6 ammonia molecules are seen to fluctuate from 0.006 to 0.05.

From the earlier research of investigation the relevance between hydrogen bonding number and cluster polarizability,[58,91] we have fitted the calculated isotropic mean polarizability values as a linear function of cluster size n, $\bar{n}_{O-H}$ and $\bar{n}_{N-H}$:

$$\bar{\alpha} = a + b \times n + c \times \bar{n}_{O-H} + d \times \bar{n}_{N-H}$$

where $n_{O-H} = \frac{n_{O-H}}{n}$ and $\bar{n}_{N-H} = \frac{n_{N-H}}{n}$ respectively represent the average O–H

hydrogen bonding number and N–H hydrogen bonding number. The fit is found to be excellent with a correlation efficient as 0.99993. It indicates that the O–H hydrogen bonds and N–H hydrogen bonds both contribute to the cluster polarizability.

CONCLUSION

In the present study, we investigated the formation of common organic oxalic acid with ammonia and their hydrogen bonded complexes using DFT calculations. The structure of $(H_2C_2O_4)(NH_3)$ agreed well with earlier reports, the ionization events and clusters growth are also studied. The present study leads to these findings:

(a) $(H_2C_2O_4)(NH_3)_n$ (n=1~6) clusters exhibit very strong hydrogen bond, in other words, oxalic acid interacts strongly with ammonia. From the analyses of bond length, interaction energy and electron density, indicating that three ammonia molecules are needed to ionize oxalic acid, forming an ion pair $HC_2O_4^-/NH_4^+$.

(b) Thermodynamics and concentration indicate oxalic acid probably form clusters with ammonia in the atmosphere. The Gibbs free energy of the global minima at different temperatures indicates that oxalic and ammonia clusters may form more favorable under the condition of low temperature. Analyzing the contributions of various isomers to the conformational population, the configurations with the lowest energy are observed with higher concentration than other isomers in the same size. Thus the small populations of the configuration with lower energy can almost be ignored. The $(H_2C_2O_4)(NH_3)$ clusters with a obvious concentration are predicted to be present in atmosphere, they could likely participate in the process of new particle formation. However, the concentrations of clusters gradually

decrease while binding more ammonia molecules. Especially from n=4, clusters show infinitesimal populations at typical boundary layer atmospheric temperatures, this could be due to the relative lower concentration of ammonia than oxalic acid in the atmosphere.

(c) Our study serves as the first scattering investigation of relevance to $(H_2C_2O_4)(NH_3)_n$ (n = 1~6) clusters. We found that the Rayleigh scattering intensities and the isotropic mean polarizabilities depend on the ammonia molecule number. Besides, the hydrogen bonds are also found to contribute to the cluster polarizability. The impact of ammonia and ammonium molecules on the subsequent nucleation of oxalic acid in Rayleigh scattering activities needs to be further studied.

The current work is fundamental and necessary for our further study of the pre-nucleation clusters containing a mixture of oxalic acid, ammonia, ammonium, water and sulfuric acid. This work predicts the possible forms of oxalic acid with ammonia when participating in nucleation in a theoretical approach, and more theoretical and experimental studies are still needed to elucidate the nucleation mechanism.

ASSOCIATED CONTENT

Supporting Information

The coordinates, harmonic frequencies (in cm^{-1}) and IR intensities for $(H_2C_2O_4)(NH_3)_n$ (n=1~6) isomers optimized by PW91PW91/6-311++G(3df,3pd)

theory of level, and the information of isomers with ammonia binding to either carboxyl and with the relative single point energy above 6 kcal mol^{-1}.

ACKNOWLEDGMENTS

The study was supported by grants from the National Natural Science Foundation of China (Grant No. 21403244 and 21133008), the National High Technology Research and Development Program of China (863 Program) (Grant No. 2014AA06A501). "Interdisciplinary and Cooperative Team" of CAS. Acknowledgement is also made to the "Thousand Youth Talents Plan". The computation was performed in EMSL, a national scientific user facility sponsored by the department of Energy's Office of Biological and Environmental Research and located at Pacific Northwest National Laboratory (PNNL). PNNL is a multiprogram national laboratory operated for the DOE by Battelle. Part of the computation was performed at the Supercomputing Center of the Chinese Academy of Sciences and Supercomputing Center of USTC.

References

1 R. J. Charlson, S. Schwartz, J. Hales, R. D. Cess, j. J. COAKLEY, J. Hansen and D. Hofmann, *Science,* 1992, **255**, 423-430.

2 M. Kulmala, H. Vehkamäki, T. Petäjä, M. Dal Maso, A. Lauri, V.-M. Kerminen, W. Birmili and P. H. McMurry, *J. Aerosol. Sci.,* 2004, **35**, 143-176.

3 G. Oberdörster and M. Utell, *Environ. Health Perspect.*, 2002, **110**, A440.

4 D. B. Kittelson, W. Watts and J. Johnson, *Atmos. Environ.*, 2004, **38**, 9-19.

5 A. Saxon and D. Diaz-Sanchez, *Nat. Immunol.*, 2005, **6**, 223-226.

6 W. Xu and R. Zhang, *J. Phys. Chem. A*, 2012, **116**, 4539-4550.

7 B. R. Bzdek and M. V. Johnston, *Anal. Chem.,* 2010, **82**, 7871-7878.

8 T. Kurtén, T. Petäjä, J. Smith, I. Ortega, M. Sipilä, H. Junninen, M. Ehn, H. Vehkamäki, L. Mauldin and D. Worsnop, *Atmos. Chem. Phys.*, 2011, **11**, 3007-3019.
9 J. Almeida, S. Schobesberger, A. Kürten, I. K. Ortega, O. Kupiainen-Määttä, A. P. Praplan, A. Adamov, A. Amorim, F. Bianchi and M. Breitenlechner, *Nature,* 2013, **502**, 359-363.
10 H. Keskinen, A. Virtanen, J. Joutsensaari, G. Tsagkogeorgas, J. Duplissy, S. Schobesberger, M. Gysel, F. Riccobono, J. G. Slowik and F. Bianchi, *Atmos. Chem. Phys.*, 2013, **13**, 5587-5600.
11 T. Jokinen, M. Sipilä, H. Junninen, M. Ehn, G. Lönn, J. Hakala, T. Petäjä, R. Mauldin III, M. Kulmala, D. Worsnop, *Atmos. Chem. Phys.*, 2012, **12**, 4117-4125.
12 K. D. Froyd and E. R. Lovejoy, *J. Phys. Chem. A*, 2011, **116**, 5886-5899.
13 T. I. Yacovitch, N. Heine, C. Brieger, T. Wende, C. Hock, D. M. Neumark and K. R. Asmis, *J. Phys. Chem. A*, 2013, **117**, 7081-7090.
14 H. R. Leverentz, J. I. Siepmann, D. G. Truhlar, V. Loukonen and H. Vehkamäki, *J. Phys. Chem. A*, 2013, **117**, 3819-3825.
15 O. Kupiainen, I. Ortega, T. Kurtén and H. Vehkamäki, *Atmos. Chem. Phys.*, 2012, **12**, 3591-3599.
16 J. Elm, M. Fard, M. Bilde and K. V. Mikkelsen, *J. Phys. Chem. A*, 2013, **117**, 12990-12997.
17 P. Paasonen, T. Olenius, O. Kupiainen, T. Kurtén, T. Petäjä, W. Birmili, A. Hamed, M. Hu and L. Huey, *Atmos. Chem. Phys.*, 2012, **12**, 9113-9133.
18 J. Wang and A. S. Wexler, *Geophys. Res. Lett.*, 2013, **40**, 2834-2838.
19 J. Elm, M. Bilde and K. V. Mikkelsen, *J. Chem. Theory Comput.,* 2012, **8**, 2071-2077.
20 J. Elm, M. Bilde and K. V. Mikkelsen, *Phys. Chem. Chem. Phys.*, 2013, **15**, 16442-16445.
21 Rozenberg, M.; Loewenschuss, A.; Nielsen, C. J. *J. Phys. Chem. A*, 2014, **118**, 1004-1011.
22 R. Zhang, *Science,* 2010, **328**, 1366-1367.
23 L. Wang, A. F. Khalizov, J. Zheng, W. Xu, Y. Ma, V. Lal and R. Zhang, *Nat. Geosci.,* 2010, **3**, 238-242.
24 R. Zhang, A. Khalizov, L. Wang, M. Hu and W. Xu, *Chem. Rev.,* 2011, **112**, 1957-2011.
25 D. Yue, M. Hu, R. Zhang, Z. Wang, J. Zheng, Z. Wu, A. Wiedensohler, L. He, X. Huang, T. Zhu, *Atmos. Chem. Phys.*, 2010, **10**, 4953-4960.
26 B. Temelso, T. N. Phan and G. C. Shields, *J. Phys. Chem. A*, 2012, **116**, 9745-9758.
27 A. J. Prenni, P. J. DeMott, S. M. Kreidenweis, D. E. Sherman, L. M. Russell and Y. *J.* Ming, *Phys. Chem. A*, 2001, **105**, 11240-11248.
28 B. Zobrist, C. Marcolli, T. Koop, B. Luo, D. Murphy, U. Lohmann, A. Zardini, U. Krieger, T. Corti and D. Cziczo, *Atmos. Chem. Phys.*, 2006, **6**, 3115-3129.
29 B. Kärcher and T. Koop, *Atmos. Chem. Phys.*, 2005, **5**, 703-714.
30 R. Wagner, O. Möhler, H. Saathoff, M. Schnaiter and T. Leisner, *Atmos. Chem. Phys.*, 2011, **11**, 2083-2110.
31 H. Giebl, A. Berner, G. Reischl, H. Puxbaum, A. Kasper-Giebl and R. Hitzenberger, *J. Aerosol. Sci.*, 2002, **33**, 1623-1634.
32 F. Yu and R. P. Turco, *Geophys. Res. Lett.*, 2000, **27**, 883-886.
33 A. B. Nadykto and F. Yu, *Phys. Rev. Lett.*, 2004, **93**, 016101.
34 Y. Xu, A. B. Nadykto, F. Yu, J. Herb and W. Wang, *J. Phys. Chem. A*, 2009, **114**, 387-396.
35 R. Zhang, L. Wang, A. F. Khalizov, J. Zhao, J. Zheng, R. L. McGraw and L. T. Molina, *Proc. Natl. Acad. Sci.*, 2009, **106**, 17650-17654.
36 A. B. Nadykto and F. Yu, *Chem. Phys. Lett.,* 2007, **435**, 14-18.
37 Y. Yokouchi and Y. Ambe, *Atmos. Environ., (1967)* 1986, **20**, 1727-1734.

38 K. Kawamura and K. Ikushima, *Environ. Sci. Technol.,* 1993, **27**, 2227-2235.
39 H. A. Khwaja, *Atmos. Environ.*, 1995, **29**, 127-139.
40 K. Kawamura, H. Kasukabe and L. A. Barrie, *Atmos. Environ.*, 1996, **30**, 1709-1722.
41 X.-F. Huang, M. Hu, L.-Y. He and X.-Y. Tang, *Atmos. Environ.*, 2005, **39**, 2819-2827.
42 P. K. Martinelango, P. K. Dasgupta and R. S. Al-Horr, *Atmos. Environ.*, 2007, **41**, 4258-4269.
43 P. Liu, W. Leaitch, C. Banic, S. M. Li, D. Ngo and W. Megaw, *J. Geophys. Res., (1984–2012)* 1996, **101**, 28971-28990.
44 Y. Xu, A. B. Nadykto, F. Yu, L. Jiang and W. Wang, *J. Mol. Struct.:THEOCHEM.*, 2010, **951**, 28-33.
45 K. H. Weber, F. J. Morales and F.-M. Tao, *J. Phys. Chem. A*, 2012, **116**, 11601-11617.
46 K. H. Weber, Q. Liu and F.-M. Tao, *J. Phys. Chem. A*, 2014, **118**, 1451-1468.
47 J.-W. Yoon, J.-H. Park, C.-C. Shur and S.-B. Jung, *Microelectron. Eng.*, 2007, **84**, 2552-2557.
48 D. J. Wales and J. P. Doye, *J. Phys. Chem. A*, 1997, **101**, 5111-5116.
49 W. Huang, R. Pal, L.-M. Wang, X. C. Zeng and L.-S. Wang, *J. Chem. Phys.*, 2010, **132**, 054305.
50 L.-M. Wang, R. Pal, W. Huang, X. C. Zeng and L.-S. Wang, *J. Chem. Phys.*, 2010, **132**, 114306.
51 W. Huang, H.-J. Zhai and L.-S. Wang, *J. Amer. Chem. Soc.*, 2010, ***132***, 4344-4351.
52 W. Huang and L.-S. Wang, *Phys. Rev. Lett.*, 2009, **102**, 153401.
53 W. Huang, M. Ji, C.-D. Dong, X. Gu, L.-M. Wang, X. G. Gong and L.-S. Wang, *ACS nano*, 2008, **2**, 897-904.
54 W. Huang, A. P. Sergeeva, H.-J. Zhai, B. B. Averkiev, L.-S. Wang and A. I. Boldyrev, *Nat. Chem.*, 2010, **2**, 202-206.
55 L.-L. Yan, Y.-R. Liu, T. Huang, S. Jiang, H. Wen, Y.-B. Gai, W.-J. Zhang and W. Huang, *J. Chem. Phys.*, 2013, **139**, 244312.
56 Y.-R. Liu, H. Wen, T. Huang, X.-X. Lin, Y.-B. Gai, C.-J. Hu, W.-J. Zhang and W. Huang, *J. Phys. Chem. A*, 2014, **118**, 508-516.
57 S. Jiang, Y. R. Liu, T. Huang, H. Wen, K. M. Xu, W. X. Zhao, W. J. Zhang and W. Huang, *J. Comput. Chem.*, 2014, **35**, 159-165.
58 S. Jiang, T. Huang, Y.-R. Liu, K.-M. Xu, Y. Zhang, Y.-Z. Lv and W. Huang, *Phys. Chem. Chem. Phys.*, 2014, **16**, 19241-19249.
59 B. Delley, *J. Phys. Chem. A*, 1990, **92**, 508-517.
60 H. Wen, Y. R. Liu, K. M. Xu, T. Huang, C. J. Hu, W. J. Zhang and W. Huang, *Chin. J. Chem. Phys.*, 2013, **26**, 729-738.
61 K.-M. Xu, T. Huang, H. Wen, Y.-R. Liu, Y.-B. Gai, W.-J. Zhang and W. Huang, *RSC Advances*, 2013, **3**, 24492-24502.
62 Y.-P. Zhu, ; Y.-R. Liu, ; T. Huang, ; S. Jiang, ; K.-M. Xu, ; H. Wen, ; W.-J. Zhang, ; W. Huang, *J. Phys. Chem. A*, 2014, **118**, 7959-7974.
63 M. Frisch, G. Trucks, H. B. Schlegel, G. Scuseria, M. Robb, J. Cheeseman, G. Scalmani, V. Barone, B. Mennucci and G. Petersson, Gaussian 09, Revision A. 02, Gaussian. *Inc., Wallingford, CT*, 2009, **200**.
64 Werner, H. J.; Knowles, P. J.; Knizia, G.; Manby, F. R.; Schütz, *Wiley Interdiscip. Rev.: Comput. Mol. Sci.*, 2012, **2**, 242-253.
65 H. Werner, P. Knowles, G. Knizia, F. Manby, M. Schütz, P. Celani, T. Korona, R. Lindh, A. Mitrushenkov and G. Rauhut, MOLPRO, version 2010.1, *a package of ab initio programs*.
66 R. F. W. Bader, Atoms in Molecules: A Quantum Theory; Oxford University Press: Oxford, U.K., 1990.

67 T. Lu, *Multiwfn: A Multifunctional Wavefunction Analyzer, Version 3.0.1*, 2013. <Http://Multiwfn.Codeplex.Com>.

68 W. Humphrey, A. Dalke and K. Schulten, VMD: visual molecular dynamics. *J. Mol. Graph.*, 1996, **14**, 33-38. <http://www.ks.uiuc.edu/Research/vmd/>.

69 E. R. Johnson, S. Keinan, P. Mori-Sanchez, J. Contreras-Garcia, A. J. Cohen and W. Yang, *J. Amer. Chem. Soc.*, 2010, **132**, 6498-6506.

70 J. Elm, P. Norman, M. Bilde and K. V. Mikkelsen, *Phys. Chem. Chem. Phys.*, 2014, **16**, 10883-10890.

71 J. Kauczor, P. Norman and W. A. Saidi, *J. Chem. Phys.*, 2013, **138**, 114107.

72 P. A. Limacher, K. V. Mikkelsen and H. P. Lüthi, *J. Chem. Phys.*, 2009, **130**, 194114.

73 P. Lind, M. Carlsson, B. Eliasson, E. Glimsdal, M. Lindgren, C. Lopes, L. Boman and P. Norman, *Mol. Phys.*, 2009, **107**, 629-641.

74 H. Solheim, K. Ruud, S. Coriani and P. Norman, *J. Chem. Phys.*, 2008, **128**, 094103.

75 T. Fahleson, J. Kauczor, P. Norman and S. Coriani, *Mol. Phys.*, 2013, **111**, 1401-1404.

76 B. F. Milne, P. Norman, F. Nogueira and C. Cardoso, *Phys. Chem. Chem. Phys.*, 2013, **15**, 14814-14822.

77 D. Cremer and E. Kraka, *Angew. Chem., Int. Ed.*, 1984, **23**, 627-628.

78 N. Han, Y. Zeng, X. Li, S. Zheng and L. Meng, *J. Phys. Chem. A*, 2013, **117**, 12959-12968.

79 U. Koch and P. Popelier, *J. Phys. Chem.*, 1995, **99**, 9747-9754.

80 J. Contreras-García, W. Yang and E. R. Johnson, *J. Phys. Chem. A*, 2011, **115**, 12983-12990.

81 A. J. Cohen, P. Mori-Sánchez and W. Yang, *Science,* 2008, **321**, 792-794.

82 X. Yang, L. Gan, L. Han, E. Wang and J. Wang, *Angew. Chem.,* 2013, **125**, 2076-2080.

83 J. H. Seinfeld and S. N. Pandis, Hoboken，New Jersey: John Wiley ＆ Sons Inc，2012: 691-711.

84 Y. Chan, R. Simpson, G. H. McTainsh, P. D. Vowles, D. Cohen and G. Bailey, *Atmos. Environ.*, 1999, **33**, 3237-3250.

85 J. Strutt, *Philos. Mag.*,1871, **41**, 107-120, 274-279.

86 J. Strutt, *Philos. Mag.*,1881, **12**, 81-101.

87 E. Rissi, E. E. Fileti and S. Canuto, *Theor. Chem. Acc.,* 2003, **110**, 360-366.

88 E. E. Fileti, ; R. Rivelino, ; S. Canuto, *J. Phys. B: At., Mol. Opt. Phys.*, 2003, **36**, 399.

89 P. Chaudhuri and S. Canuto, *J. Mol. Struct.:THEOCHEM.*, 2006, **760**, 15-20.

90 E. Orestes, P. Chaudhuri and S. Canuto, *Mol. Phys.*, 2012, **110**, 297-306.

91 T. K. Ghanty and S. K. Ghosh, *J. Chem. Phys.*, 2003, **118**, 8547–8550.

Table 1. Calculated Gibbs free energy and free energy changes of NH_3, $C_2O_2H_4$, $(C_2O_2H_4)(NH_3)$ and $(C_2O_2H_4)(NH_3)_2$ using different DFT functional with 6-311++G(3df,3pd) basis set.

Isomer	Functional	G(Hatree)	ΔG (kcal mol^{-1})
NH3	ωB97x-D	-56.550	
	M06-2X	-56.536	
	CAM-B3LYP	-56.541	
	B3LYP	-56.572	
	PW91PW91	-56.544	
C2O2H4	ωB97x-D	-378.337	
	M06-2X	-378.321	
	CAM-B3LYP	-378.333	
	B3LYP	-378.462	
	PW91PW91	-378.363	
(C2O2H4)(NH3)	ωB97x-D	-434.891	-2.422
	M06-2X	-434.862	-3.324
	CAM-B3LYP	-434.891	-10.309
	B3LYP	-435.037	-1.420
	PW91PW91	-434.914	-4.172
(C2O2H4)(NH3)2	ωB97x-D	-491.435	0.988
	M06-2X	-491.393	-0.660
	CAM-B3LYP	-491.413	1.517
	B3LYP	-491.602	3.165
	PW91PW91	-491.455	-2.300

Table 2. Calculated isotropic mean polarizabilities ($\bar{\alpha}$) of NH_3, $C_2O_2H_4$, $(C_2O_2H_4)(NH_3)$ and $(C_2O_2H_4)(NH_3)_2$ using different DFT functional with aug-cc-pVDZ basis set.

Functional	NH_3	$C_2O_2H_4$	$(C_2O_2H_4)(NH_3)$	$(C_2O_2H_4)(NH_3)_2$
ωB97x-D	13.980	38.651	53.682	68.472
M06-2X	13.645	37.675	52.551	67.032
CAM-B3LYP	14.000	38.663	53.814	68.935
MP2	14.041	39.984	55.492	70.855
PW91PW91	14.993	41.795	58.532	75.362

Table 3. The relative single point energy ΔE_{rel}, the ZPE-corrected binding energies (ΔE_0), intermolecular enthalpy (ΔH), free energy changes (ΔG) and Boltzmann averaged Gibbs free energy of $(H_2C_2O_4)(NH_3)_n$ (n = 1~6) (in kcal mol^{-1}) based on PW91PW91/6-311++G(3df,3pd) calculations.

n	isomer	ΔE_{rel}	ΔE_0	ΔH	ΔG	Boltzmann averaged Gibbs free energy
1	I -a	0	-14.094	-14.612	-5.147	-5.147
2	II -a	0	-20.539	-21.630	-2.404	-0.797
	II -b	4.807	-15.732	-15.984	0.821	
3	III -a	0	-34.158	-36.219	-6.018	-4.447
	III -b	0.191	-33.966	-35.783	-5.689	
	III -c	0.430	-33.728	-35.755	-6.297	
	III -d	0.820	-33.338	-35.439	-5.671	
	III-e	5.670	-28.459	-29.893	-1.405	
	III-f	6.032	-28.126	-29.269	1.558	
4	IV -a	0	-37.308	-38.756	-1.449	5.284
	IV -b	0.747	-36.561	-38.001	-0.911	
	IV -c	0.895	-36.413	-38.333	-0.264	
	IV -d	2.710	-34.599	-36.395	1.594	
	IV -e	3.425	-33.883	-35.482	1.931	
	IV -f	3.834	-33.474	-35.271	3.018	
	IV -g	4.415	-32.893	-34.804	3.628	

	IV -h	5.190	-32.119	-33.991	3.405	
5	V -a	0	-44.356	-46.262	0.522	2.927
	V -b	0.708	-43.649	-45.712	1.749	
	V -c	1.040	-43.316	-45.413	1.595	
	V -d	1.232	-43.125	-44.954	1.501	
	V -e	1.895	-42.461	-44.601	2.377	
	V -f	2.209	-42.147	-44.560	4.416	
	V -g	2.531	-41.825	-44.488	5.360	
	V -h	3.772	-40.584	-42.668	3.470	
	V -i	4.031	-40.326	-42.694	5.744	
6	VI -a	0	-51.544	-54.332	3.495	12.667
	VI -b	1.808	-49.736	-52.098	4.483	
	VI -c	3.540	-48.004	-50.898	8.164	
	VI -d	4.697	-46.847	-49.662	8.886	
	VI -e	5.569	-45.975	-48.680	8.984	
	VI -f	5.975	-45.568	-48.295	9.129	

Table 4. Topological parameters at intermolecular bond critical points (BCPs) between oxalic acid and ammonia of all global minima at PW91PW91/6-311++G(3df,3pd) level. The subscripts are used to mark the carbon atoms of different carbonyl.

isomer	BCP	ρ	$\nabla^2\rho$	E	G	V	−G/V
I-a	$HOOC_1C_2OO$-H···NH_3	0.0853	0.0136	-0.0400	0.0434	-0.0835	0.52
	NH_2-H···$OHOC_1C_2OOH$	0.0178	0.0668	0.0024	0.0143	-0.0118	1.21
II-a	$HOOC_1C_2OO$···H-NH_3NH_3	0.1359	-0.0796	-0.0967	0.0768	-0.1735	0.44
	NH_3NH_2-H···$OHOC_1C_2OOH$	0.0106	0.0394	0.0012	0.0086	-0.0074	1.16
III-a	$HOOC_1C_2OO$···H-$NH_3(NH_3)_2$	0.0742	0.1013	-0.0263	0.0516	-0.0779	0.66
	$(NH_3)_2NH_2$-H···$OHOC_1C_2OOH$	0.0192	0.0769	0.0028	0.0164	-0.0135	1.21
	$(NH_3)_2NH_2$-H···$OHOC_1C_2OOH$	0.0146	0.0538	0.0021	0.0113	-0.0092	1.23
IV-a	$HOOC_1C_2OO$···H-$NH_3(NH_3)_3$	0.0645	0.1069	-0.0197	0.0464	-0.0661	0.70
	$(NH_3)_3NH_2$-H···$OHOC_1C_2OOH$	0.0136	0.0503	0.0020	0.0105	-0.0085	1.24
	$(NH_3)_3NH_2$-H···$OHOC_1C_2OOH$	0.0136	0.0503	0.0020	0.0105	-0.0085	1.24
	$(NH_3)_3NH_2$-H···$OHOC_1C_2OOH$	0.0129	0.0488	0.0021	0.0101	-0.0081	1.25
V-a	$HOOC_1C_2OO$···H-$NH_3(NH_3)_4$	0.0473	0.1087	-0.0082	0.0354	-0.0436	0.81
	$(NH_3)_4NH_2$-H···$OHOC_1C_2OOH$	0.0225	0.0748	0.0015	0.0172	-0.0158	1.09
	$(NH_3)_4NH_2$-H···$OHOC_1C_2OOH$	0.0180	0.0741	0.0029	0.0156	-0.0127	1.23
	$(NH_3)_4NH_2$-H···$OHOC_1C_2OOH$	0.0131	0.0461	0.0017	0.0098	-0.0081	1.21
VI-a	$HOOC_1C_2OO$···H-$NH_3(NH_3)_5$	0.0446	0.1054	-0.0072	0.0335	-0.0407	0.82
	$(NH_3)_5NH_2$-H···$OHOC_1C_2OOH$	0.0215	0.0717	0.0015	0.0164	-0.0149	1.10
	$(NH_3)_5NH_2$-H···$OHOC_1C_2OOH$	0.0215	0.0717	0.0015	0.0164	-0.0149	1.10
	$(NH_3)_5NH_2$-H···$OHOC_1C_2OOH$	0.0186	0.0764	0.0029	0.0161	-0.0132	1.22

Table 5. Gibbs free energy [a] values in kcal mol^{-1}, relative bound percentages [b] (RPF × 100%) and estimated concentrations for the stable clusters of $(H_2C_2O_4)(NH_3)_n$ (n=1~4). The estimated atmospheric concentrations are based on an oxalic acid concentration of 5 ppb and an ammonia concentration of 1ppb.

n	Isomers	ΔG (kcal mol^{-1})	RPF×100%	molecules cm^{-3}
1	I-a	-5.149	5.96×10^{-4}	8.02×10^{5}
2	II-a	-2.404	5.79×10^{-15}	7.79×10^{-6}
	II-b	0.821	2.50×10^{-17}	3.36×10^{-8}
3	III-a	-6.018	2.59×10^{-21}	3.49×10^{-12}
	III-b	-5.689	1.49×10^{-21}	2.00×10^{-12}
	III-c	-6.297	4.16×10^{-21}	5.59×10^{-12}
	III-d	-5.671	1.44×10^{-21}	1.94×10^{-12}
	III-e	-1.405	1.07×10^{-24}	1.44×10^{-15}
	III-f	-1.558	1.39×10^{-24}	1.87×10^{-15}
4	IV -a	-1.449	1.16×10^{-33}	1.55×10^{-24}
	IV -b	-0.911	4.66×10^{-34}	6.27×10^{-25}
	IV -c	-0.264	1.56×10^{-34}	2.10×10^{-25}

[a] PW91PW91/6-311++G(3df,3pd) results. [b] With respect to the corresponding clusters.

Figure Captions

Fig. 1 The optimized geometries of $(H_2C_2O_4)(NH_3)_n$ (n=1~6) at the PW91PW91/6-311++G(3df,3pd) level of theory (red for oxygen, white for hydrogen, gray for carbon and blue for nitrogen).

Fig. 2 The lowest-energy structures of the $(H_2C_2O_4)(NH_3)_n$ (n=1~6) clusters at the PW91PW91/6-311++G(3df,3pd) level of theory ordered by the state of dissociation (I, II, III, IV, V, VI). The intramolecular and intermolecular interaction distances and the corresponding isosurfaces are given.

Fig. 3 The conformational population changes in the low isomers of $(H_2C_2O_4)(NH_3)_4$ as a function of temperature (OA stands for oxalic acid, AM stands for ammonia).

Fig. 4 The conformational population changes in the low isomers of $(H_2C_2O_4)(NH_3)_5$ as a function of temperature (OA stands for oxalic acid, AM stands for ammonia).

Fig. 5 The conformational population changes in the low isomers of $(H_2C_2O_4)(NH_3)_6$ as a function of temperature (OA stands for oxalic acid, AM stands for ammonia).

Fig. 6 The Gibbs free energy changes (in kcal mol^{-1}) from global minimum for the $(H_2C_2O_4)(NH_3)_n$ (n = 1~6) clusters depending on various temperature at the PW91PW91/6-311++G(3df,3pd) level of theory.

Fig. 7 The Rayleigh light scattering and cluster polarizability properties: (a) Rayleigh light scattering intensities as a function of ammonia molecules; (b) depolarization ratio as a function of ammonia molecules; (c) isotropic mean polarizabilities as a function of ammonia molecules; (d) anisotropic polarizabilities as a function of ammonia molecules.

Fig. 1

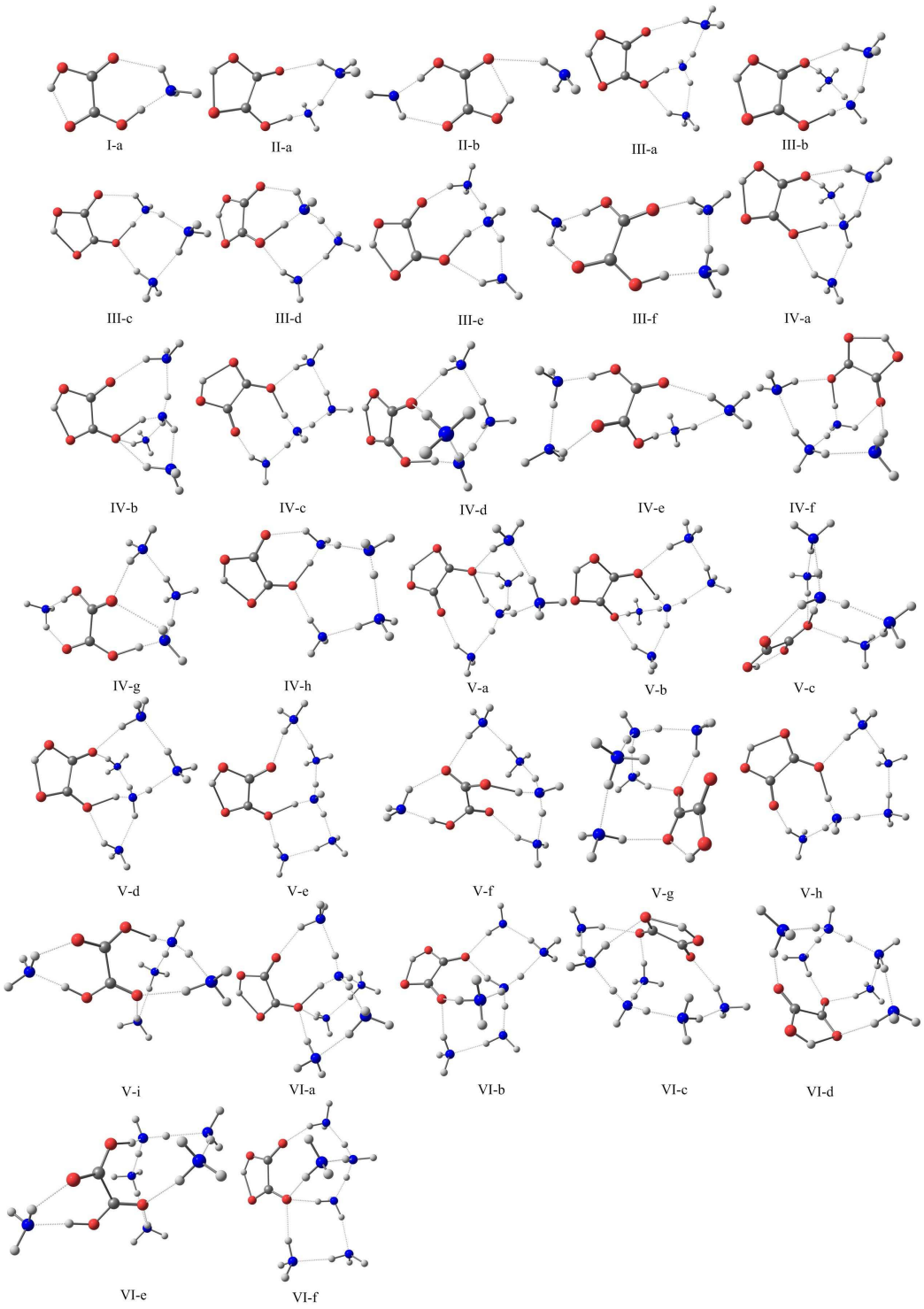

Fig. 2

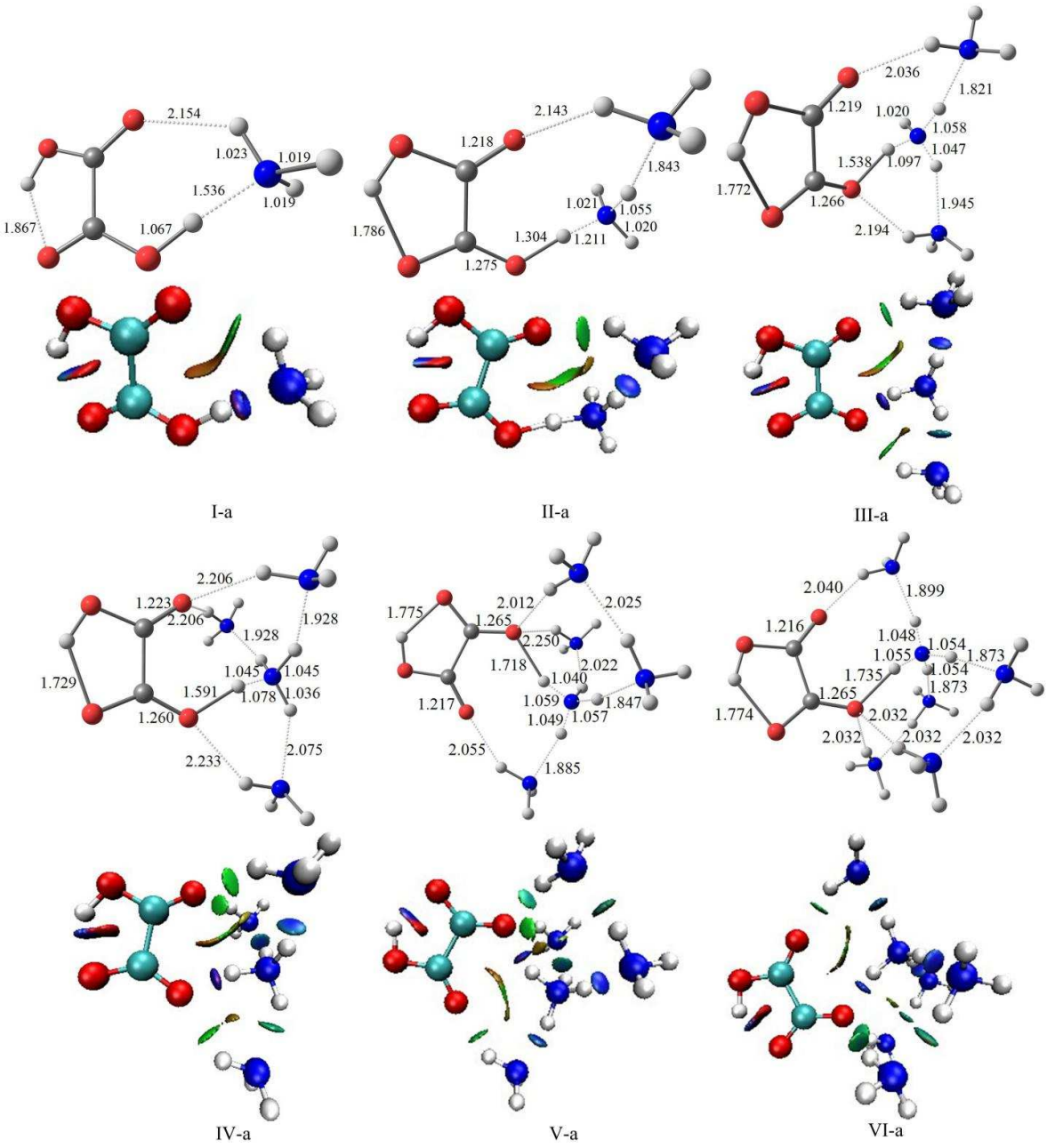

Fig. 3

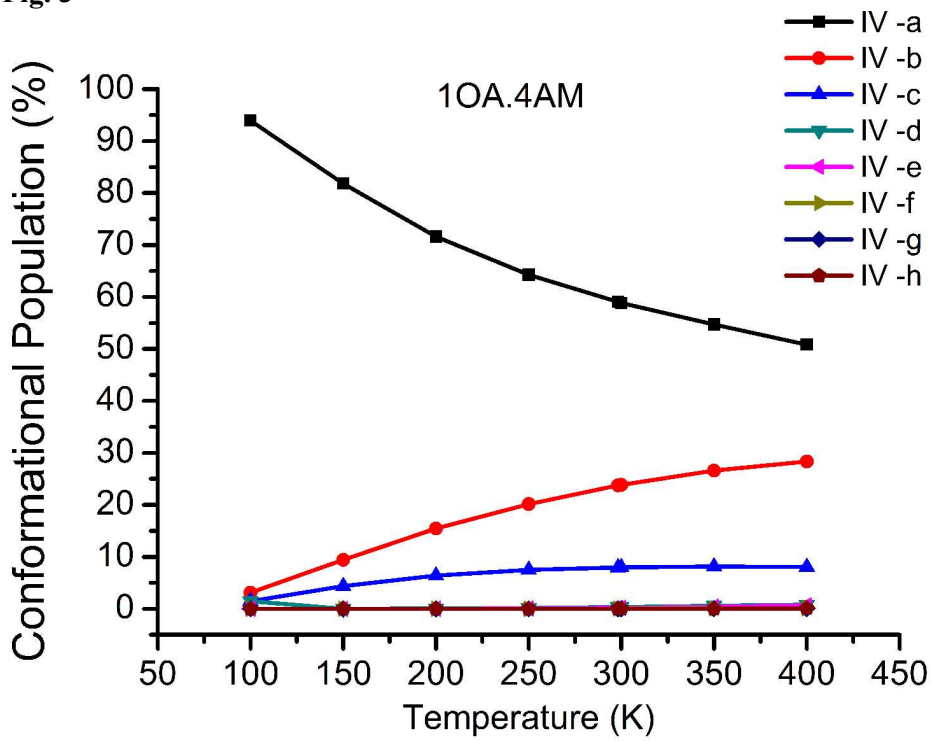

Fig. 4

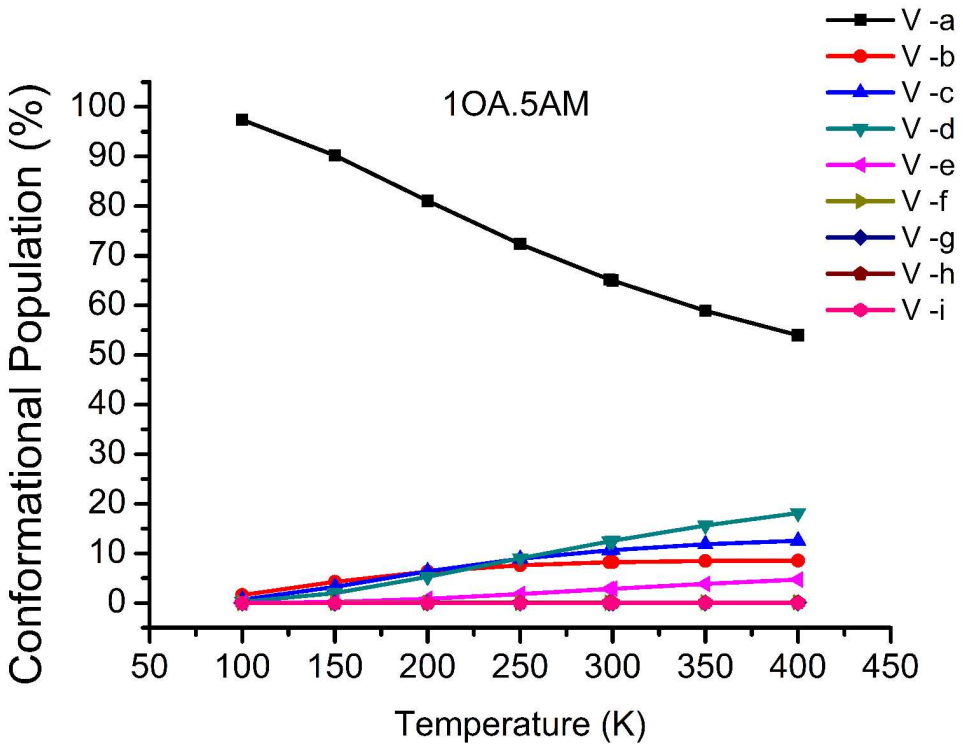

Fig. 5

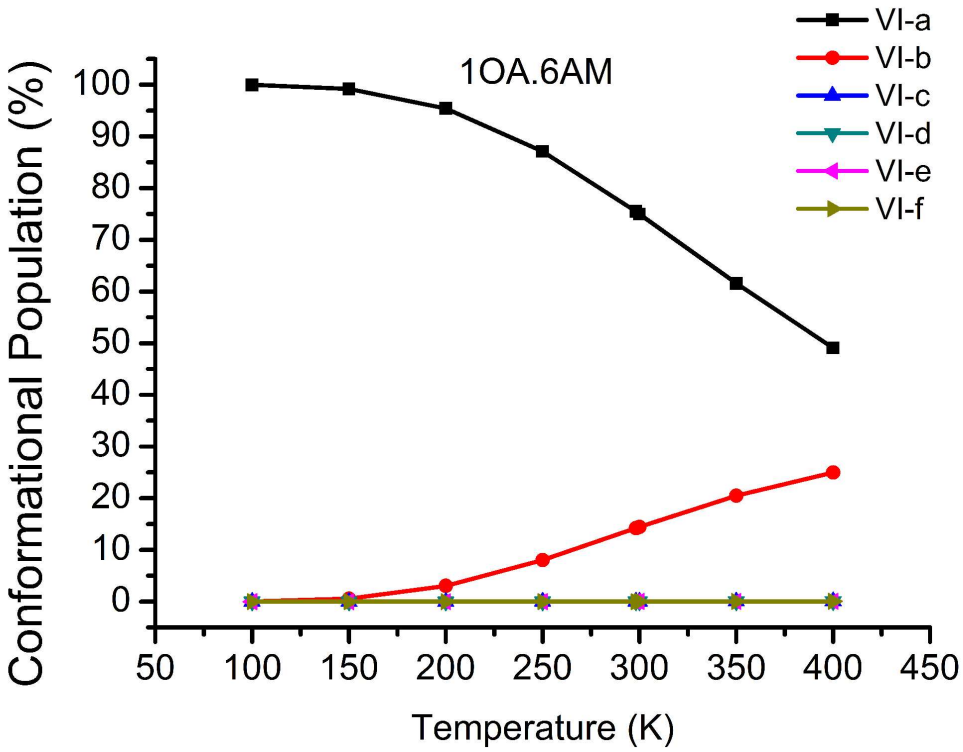

Fig. 6

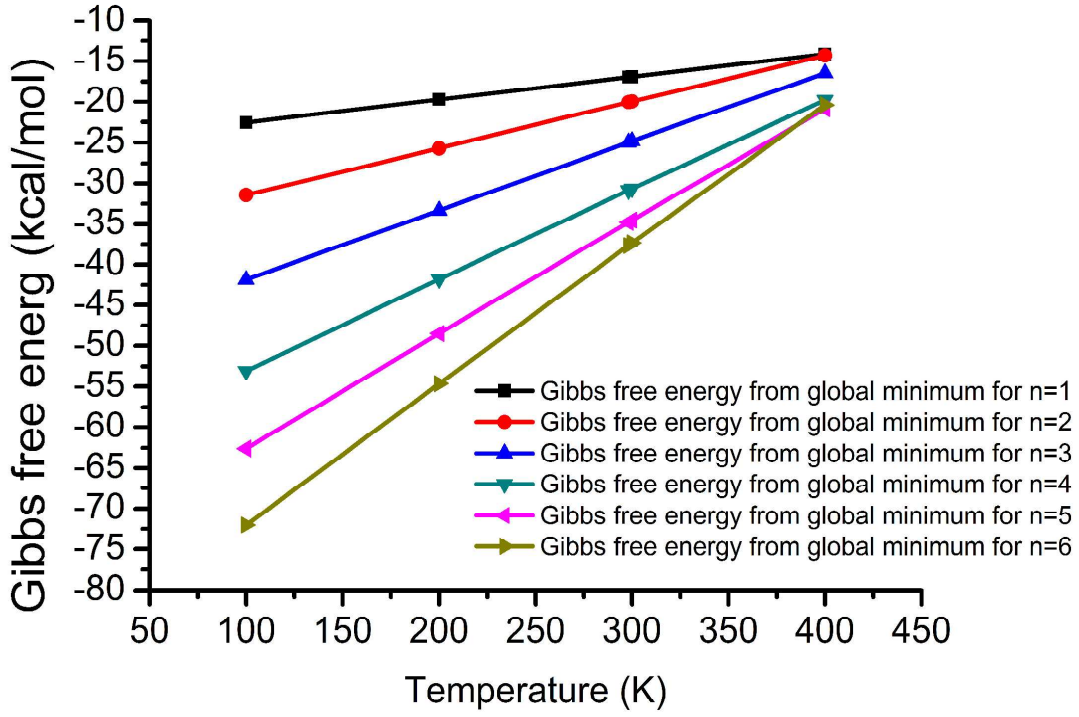

Fig. 7